

Supporting Information for Modeling in “Edge Effects Determine the Direction of Bilayer Bending”

Silas Alben¹, Bavani Balakrisnan² and Elisabeth Smela²

¹School of Mathematics, Georgia Institute of Technology, Atlanta, GA, USA, ² Department of Mechanical Engineering, University of Maryland, College Park, MD, USA

1 Model details

We now derive the expression for the elastic energy of a bilayer material in terms of its spatial configuration, given by its displacement from the initial planar state. We assume that the strain in each layer of the bilayer is given by the Föppl-von-Kármán theory of the deformation of thin plates, which is accurate for plate deflections which are comparable to the planar dimensions of the plate [2].

When the polymer layer undergoes expansion or contraction, the bilayer finds a new equilibrium state in which each material point is displaced. The displacement vector field is

$$\vec{d}(x, y, z) = (u_x(x, y, z), u_y(x, y, z), u_z(x, y, z)). \quad (1)$$

where (x, y, z) is the coordinate of the material point in the undeformed state. In this theory, the deformation of the entire bilayer is determined by the displacement of the middle surface of the substrate, which is given by:

$$u_x \Big|_{z=-h_s/2} = F(x, y); \quad u_y \Big|_{z=-h_s/2} = G(x, y); \quad u_z \Big|_{z=-h_s/2} = \zeta(x, y). \quad (2)$$

F and G represent in-plane displacements, while ζ represents out-of-plane displacement. Because the bilayer is thin, and no stresses are applied across the external z -surfaces of

the bilayer, the stresses across z -surfaces in the interior of the layer may be shown to be negligible. The corresponding strains are also zero then:

$$\begin{aligned} 0 &= \sigma_{xz} = \frac{1+\nu}{E}u_{xz} = \frac{1}{2}(\partial_x u_z + \partial_z u_x) \\ 0 &= \sigma_{yz} = \frac{1+\nu}{E}u_{yz} = \frac{1}{2}(\partial_y u_z + \partial_z u_y). \end{aligned} \quad (3)$$

Because the bilayer is thin, the z displacement is nearly constant through the z -thickness of the bilayer:

$$u_z(x, y, z) \approx \zeta(x, y). \quad (4)$$

Combining Eqs. (2), (3) and (4),

$$u_x(x, y, z) = -z\partial_x\zeta(x, y) + F(x, y); \quad u_y(x, y, z) = -z\partial_y\zeta(x, y) + G(x, y). \quad (5)$$

u_x and u_y are extension and compression on opposite sides of the middle surface due to bending, superposed on in-plane stretching. The nonzero components of the strain tensor are thus

$$u_{xx}(x, y, z) = -z\partial_{xx}\zeta + s_{xx}^{(f)}, \quad (6)$$

$$u_{xy}(x, y, z) = -z\partial_{xy}\zeta + s_{xy}, \quad (7)$$

$$u_{yy}(x, y, z) = -z\partial_{yy}\zeta + s_{yy}^{(f)}. \quad (8)$$

The in-plane strain terms $s_{xx}^{(f)}, s_{xy}, s_{yy}^{(f)}$ are given separately in the substrate and the film. The superscript f is used for values of z in the film. In the substrate, $-h_s < z < 0$, we have

$$s_{xx}(x, y) = \frac{1}{2}(\partial_x\zeta)^2 + \partial_x F, \quad (9)$$

$$s_{xy}(x, y) = \frac{1}{2}\partial_x\zeta\partial_y\zeta + \frac{1}{2}(\partial_x G + \partial_y F), \quad (10)$$

$$s_{yy}(x, y) = \frac{1}{2}(\partial_y\zeta)^2 + \partial_y G. \quad (11)$$

The effect of differential expansion in the polymer film is given by setting the equilibrium strain to a nonzero constant, ϵ_a , called the ‘‘actuation strain.’’ Thus for the film, which occupies $0 \leq z < h_f$, the two components of the in-plane strain related to volumetric expansion are

$$(s_{xx}^f, s_{yy}^f) = (s_{xx}, s_{yy}) + \epsilon_a, \quad (12)$$

while the shear strain term is the same in the film and in the substrate: $s_{xy}^f = s_{xy}$. Having derived the components of the strain tensor u_{xx} , u_{xy} , and u_{yy} for our bilayer model, the free energy per unit volume in the bilayer can be computed in terms of u_{xx} , u_{xy} , u_{yy} by the the Föppl-von-Kármán theory of the deformation of thin plates, derived in [2]). The energy densities are:

$$v_{f/s} = \frac{E_{f/s}}{2(1 + \nu_{f/s})} (u_{xx}^2 + u_{yy}^2 + 2u_{xy}^2) + \frac{\nu_{f/s}}{1 - 2\nu_{f/s}} (u_{xx}^2 + u_{yy}^2 + 2u_{xx}u_{yy}) \quad (13)$$

$$v_{f/s} = \frac{E_{f/s}}{2(1 + \nu_{f/s})} \left(\frac{1 - \nu_{f/s}}{1 - 2\nu_{f/s}} u_{xx}^2 + \frac{1 - \nu_{f/s}}{1 - 2\nu_{f/s}} u_{yy}^2 + 2u_{xy}^2 + \frac{2\nu_{f/s}}{1 - 2\nu_{f/s}} u_{xx}u_{yy} \right). \quad (14)$$

The subscript f or s is used for the film or substrate, respectively. The total free energy of the bilayer is then

$$U = U_s + U_f, \quad (15)$$

$$U_s = \int_{-W/2}^{W/2} dx \int_{-L/2}^{L/2} dy \int_{-h_s}^0 dz v_s, \quad (16)$$

$$U_f = \int_{-W/2}^{W/2} dx \int_{-L/2}^{L/2} dy \int_0^{h_f} dz v_f. \quad (17)$$

2 Comparison with experiment by Hou and Chen

We have simulated the problem of Hou and Chen in which the bilayer is clamped along one edge [1]. We have used the same geometrical parameters and material parameters as in their medium (their Figures 5 and 10), narrow (their Figures 6 and 11) and wide (their Figures 7 and 12) strips. The actuation strain is not given in their work, so we set the actuation strain to give the same maximum deflection of their medium strip. We have scaled all lengths by the bilayer length.

We found that the medium strip is doubly curved (Figure SI-1A), and the wide and narrow ones are not (Figure SI-1B-C). We also saw their edge layer for the wide strip, and the wide strip deflected about 40% more than the narrow strip, as they found.

The thickness to length ratio of Hou and Chen is about 100 times ours. We hypothesized that the double curvature of the medium aspect ratio strip would disappear at thicknesses within the range of our experiment. Hence we simulated their problem again, but decreased the thickness by a factor of 100 and the actuation strain by a factor of 100. We obtained nearly the same average deflection but with a shape which was nearly developable, as in our experiments, and not doubly curved, shown in Figure SI-1D.

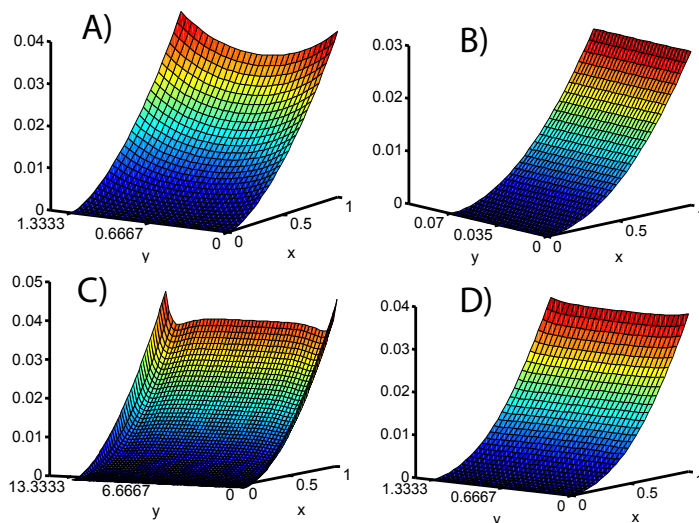


Figure 1: A) Medium width strip (aspect ratio 4/3) clamped along one edge, as in Figures 5 and 10 of [1], showing double curvature. B) Narrow strip (aspect ratio 2.1/30) and C) Wide strip (aspect ratio 400/30) under the same actuation strain as in A. D) Medium width strip as in A, but with thickness to length ratio and actuation strain decreased by factors of 100.

References

- [1] M.T.K. Hou and R. Chen. Effect of width on the stress-induced bending of micromachined bilayer cantilevers. *Journal of Micromechanics and Microengineering*, 13:141–148, 2003.
- [2] E.D. Landau and E.M. Lifshitz. *Theory of Elasticity*. Pergamon Press, Oxford, UK, 1986.

Supporting Information for Experiments in “Edge Effects Determine the Direction of Bilayer Bending”

by

Silas Alben, Bavani Balakrisnan, and Elisabeth Smela

1	Bilayer Fabrication.....	1
2	Arrays Used to Generate the Data in Figure 4 of the Main Text.....	3
3	Results from Other Samples	7
4	Y-Direction Bending < 50% for $A = 1$	10
5	Square vs. Circular Center Mount	12
6	Additional SEM Images.....	17
7	Dog-Ears	17
8	Actuation Video	19
	Supporting Information References.....	20

1 Bilayer Fabrication

A combination of differential adhesion [1] and sacrificial release methods [2] was used to fabricate polypyrrole actuators to ensure completely free movement of devices upon actuation. Partial adhesion during the first cycle changes the behavior, since it leads to the corners lifting first. The poor adhesion of SiO_2 to Au was used to advantage in the sacrificial layer removal step. Separation of the Au from the SiO_2 allows the HF wet etchant to etch from the top, rather than just the side, reducing the etch time. This is beneficial for the actuation of the PPy, which is adversely affected by HF.

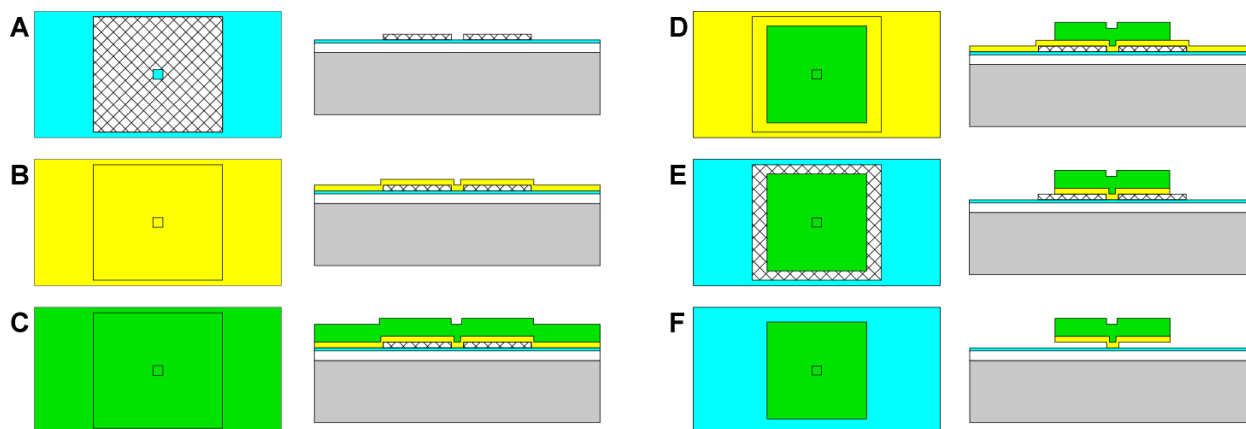


Figure SI - 1. Fabrication process for the PPy(DBS)/Au bilayer actuators. A) Onto an oxidized Si wafer, deposit a layer of Cr. Deposit and pattern a sacrificial layer of SiO₂. Deposit B) Au and C) PPy. Pattern the D) PPy and E) Au. F) Remove the sacrificial layer.

The fabrication process for the PPy(DBS)/Au bilayer actuators is shown in Figure SI - 1. A Cr adhesion layer (40 nm) and an SiO₂ sacrificial layer (100 nm) were sequentially deposited onto an oxidized Si wafer by electron beam evaporation. Positive resist (Shipley 1813) was spin-coated onto the SiO₂, exposed to 365 nm UV light in a mask aligner, and developed (Shipley 352). The SiO₂ was wet etched using buffered HF (JT Baker) diluted by a factor of 66 in deionized (DI) water. This first mask step defines the rectangular sacrificial layer area, which has 10-16 μm square openings down to the underlying Cr. The resist was removed via flood exposure and development to avoid surface residue from exposure to organic solvents. Immediately after rinsing the surface in DI and drying, the Au was deposited. Further surface treatments, such as piranha, oxygen plasma, or Cr etching, caused difficulties in later steps.

The PPy-Au bilayers were fabricated by first depositing an Au layer (100 nm) by thermal evaporation. This was followed immediately by the electrochemical deposition of a first PPy(ClO₄) adhesion layer. This was grown by cyclic voltammetry, ramping the potential between 0 and 0.6 V vs. Ag/AgCl at 50 mV/s for 2 scans in 150 mL of an aqueous solution of 0.1 M pyrrole and 0.1 M NaClO₄. Thereafter the actuating PPy(DBS) layer was deposited potentiostatically (EcoChemie AutoLab) to a thickness of 400 nm at 0.46 V vs. Ag/AgCl in 150 mL of an aqueous solution of 0.1 M pyrrole and 0.1 M NaDBS. The counter electrode was an oxidized Si wafer coated with Au (100)/Cr (20 nm) positioned parallel to the sample and 4 cm away. The reference electrode was placed close to the back side of the sample. After deposition, care was taken during rinsing and drying to prevent excessive shear forces that would delaminate the Au.

Photoresist (1813) was patterned onto the surface of the PPy to act as a mask during the dry etching of the PPy by reactive ion etching in an oxygen plasma. The photoresist was removed by continued etching in the oxygen plasma; the etch rates for the resist and the PPy are comparable. The exposed Au was removed by wet etching (Transene Au etchant, diluted 2x) without agitation. Since some of the structures were partially freed during this step, undercutting of the Au occurred with agitation. The devices were kept in DI water after the Au was patterned to

prevent stiction until the structures were released by wet etching in the dilute HF (66x) solution. The released bilayers were stored in water to prevent stiction after HF etching. Testing was performed without delay to prevent chemical reactions on the surface of the exposed Cr, which occur over time if the Cr is left in the water.

The devices were actuated in 0.1 M NaDBS (EcoChemie AutoLab). The sample and the counter electrode were both fixed flat at the bottom of an electrochemical cell, with a spacing of 0.5 cm between them. The reference electrode was adjacent to the sample. The PPy was first reduced by ramping the voltage from 0 to -0.85 V vs. Ag/AgCl at 10 mV/sec using a Au (100)/Cr (20 nm) on oxidized Si wafer counter electrode. The oxidation/reduction level was monitored by measuring the consumed current. It was then partially re-oxidized by gradually increasing the voltage in small increments until the bilayers started to curve upward (at approx. -0.63 V). The bilayers were imaged through Leica MZ12.5 stereomicroscope using Buntton 5 MP CMOS digital camera under coaxial illumination.

2 Arrays Used to Generate the Data in Figure 4 of the Main Text

The eleven arrays from which the data in Figure 4 were obtained (Sample 1) in the main text are shown in Figure SI - 2. In these images, the bilayers are in the oxidized (curled) state. Two kinds of defects that can be seen here and in the following figures: 1) devices that are missing because they sheared off (e.g. during rinsing or moving the wafer into the actuation solution) and 2) devices that did not release but that remained flat on the surface due to stiction. It is likely that stiction also led to the small number of dog-ears and corkscrews that are present. Also, not all of the devices are fully curled up. The reasons for incomplete actuation may be stiction or a poor electrical connection. If the bending direction was clear, then these were included in the counts of spirals, cigars, dog-ears, and corkscrews.

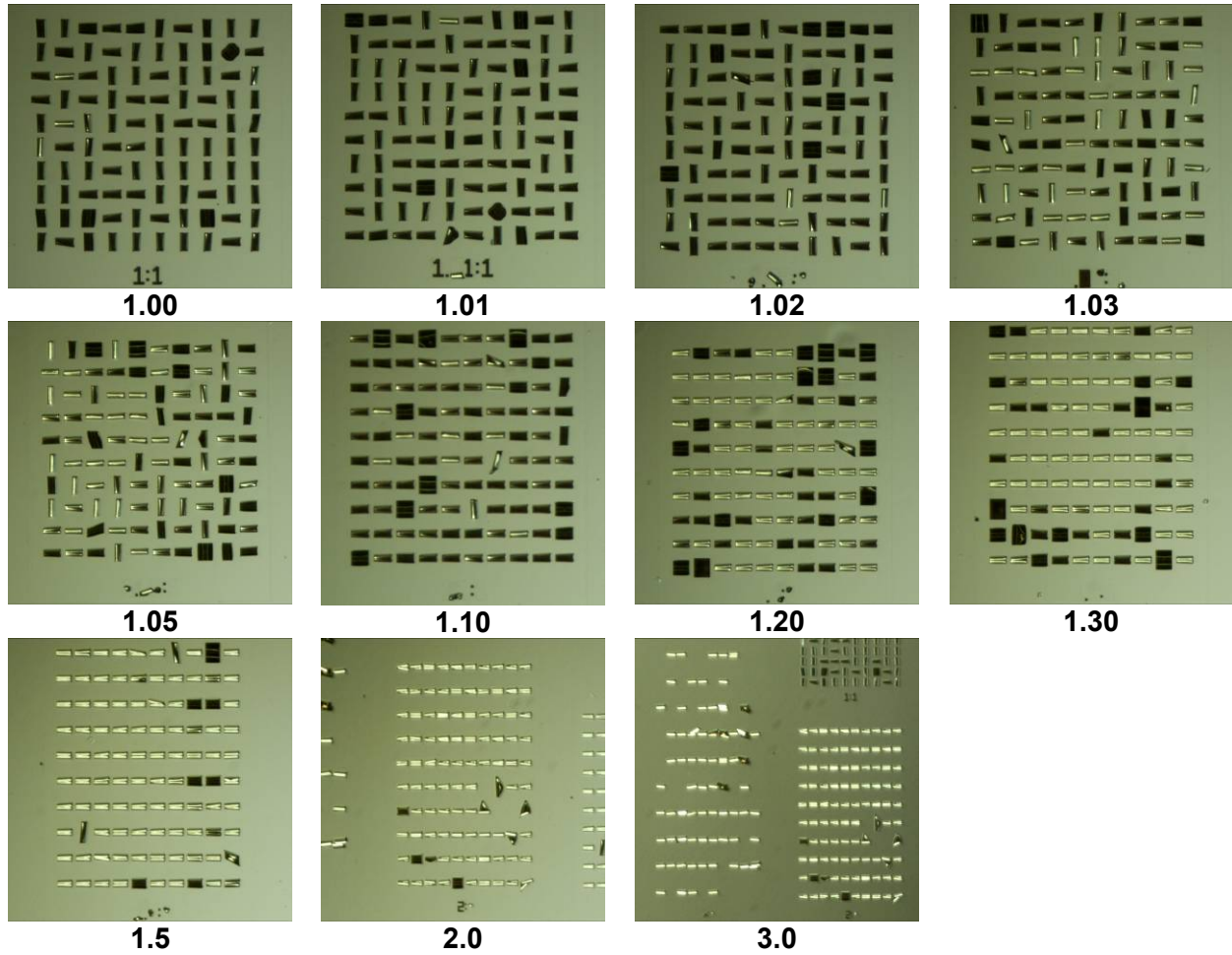
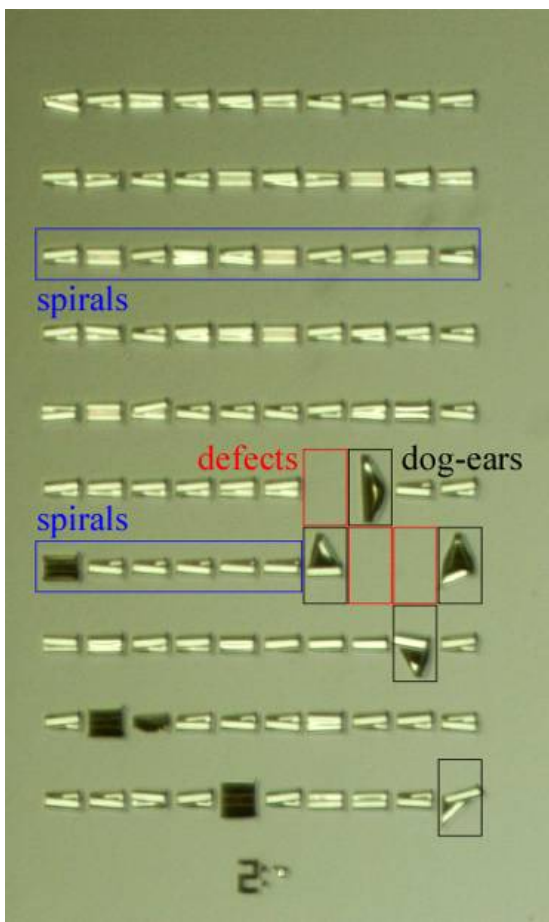


Figure SI - 2. Sample 1 arrays with increasing aspect ratio (used to generate the data in Figure 4 in the main text). Bilayers were considered defective if they came off the surface (such as in $A = 2.0$ at the position $x = 9, y = 7$), did not curl ($A = 1.2, x = 8, y = 1$), or partially adhered to the substrate ($A = 1.10, x = 7, y = 2$).

Supporting Info for Experiments in “Edge Effects Determine the Direction of Bilayer Bending”
 Alben, Balakrisnan, Smela

Close-ups of three of the arrays showing how the devices were categorized are included in Figure SI - 3 and Figure SI - 4. In Figure SI - 4b there were three defects due to stiction: the bilayers did not pick up (they were flat). In Figure SI - 4c,d it is probable, but not absolutely clear, that stiction caused the dog-eared or corkscrew bilayers, so they were counted as dog-ears or corkscrews rather than defects. Out of the 1100 bilayers in the 11 arrays, the total number of dog-ears was 11, corkscrews 13, and defects 43.



cigars	spirals	dog-ear	cork-screw	defects
0	10			
0	10			
0	10			
0	10			
0	10			
0	8	1		1
0	6	2		2
0	9	1		
0	10	1		
0	9	1		

a)

b)

Figure SI - 3. a) Sample 1, $A = 2$ array showing how the bilayers were categorized. b) The counts for each row of the array. These devices are so long that they curl into a double-spiral (see SEM images in Figure SI - 14c,d).

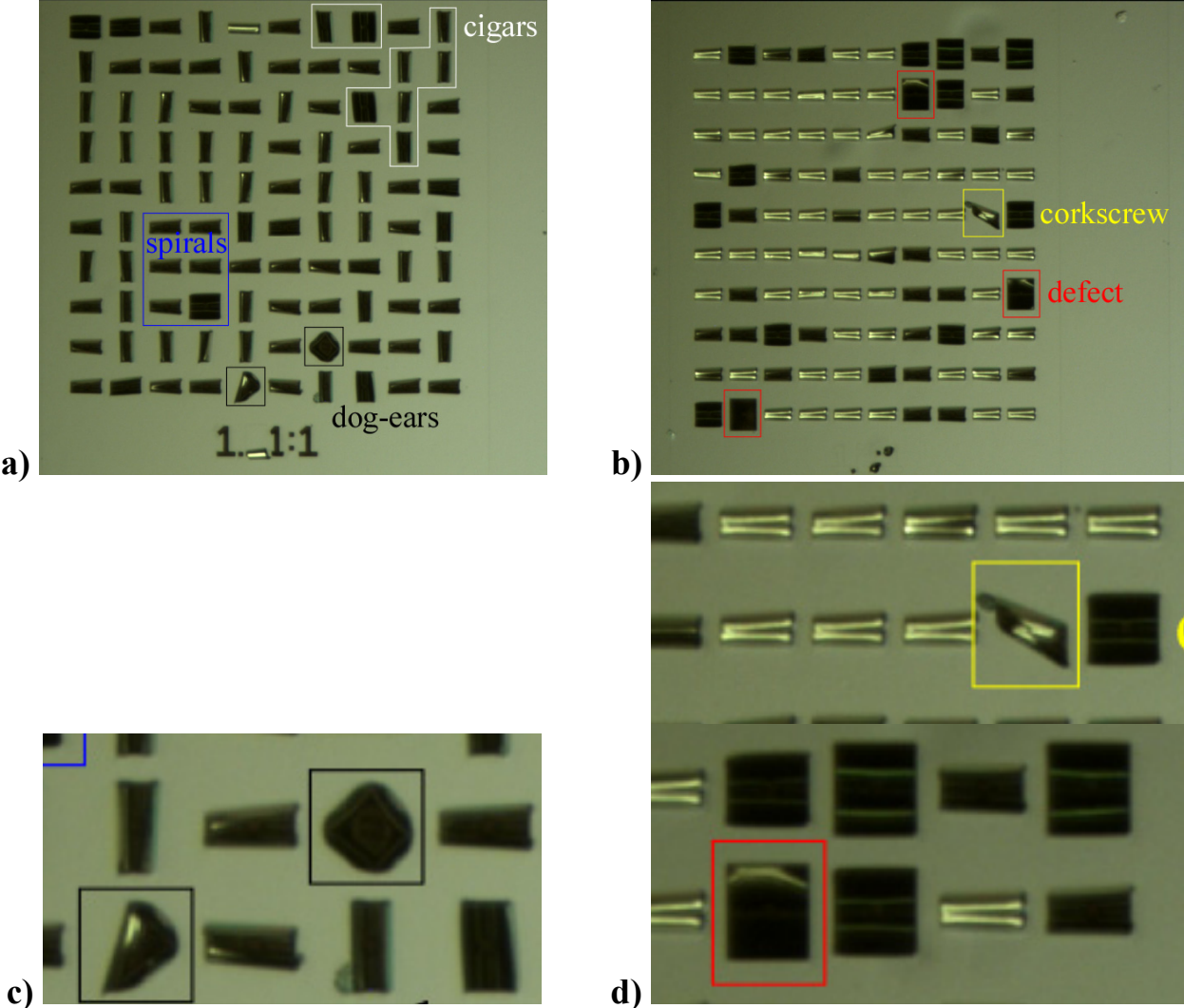


Figure SI - 4. Sample 1, a) $A = 1.01$ and b) $A = 1.2$ arrays showing how the bilayers were categorized. c) & d) close-ups from a) & b), respectively.

From the images, one can see that bilayers with larger aspect ratios had a larger number of defects (Figure SI - 5); this is because the shear forces they experienced during fabrication were larger for the bigger plates, leading to delamination. The number of bilayers with at least one dog-eared corner and those that tilted (corkscrews) are also plotted in Figure SI - 5.

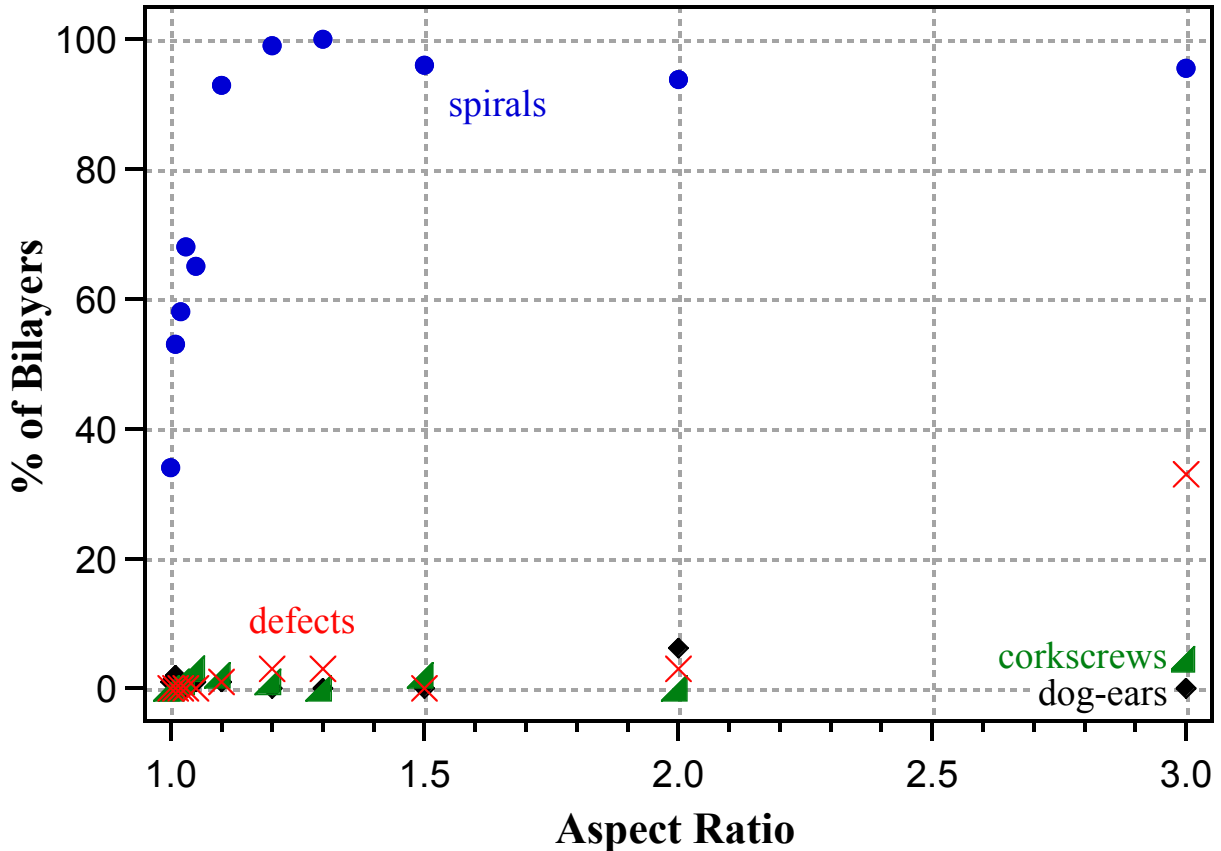


Figure SI - 5. Percentage of defect-free bilayers from Sample 1 (arrays in Figure SI - 2) with one or more corners curled inward (dog-ears) (black diamonds), spirals (blue circles), and corkscrews (green triangles). Also shown is the percentage of defective/missing bilayers (red Xs).

3 Results from Other Samples

It must be emphasized that the fabrication of perfect devices is exceedingly challenging. The slightest degree of stickiness to the surface results in dog-ears or corkscrews (the subject of a future publication). Variations in PPy thickness or a mask in which the dimensions are slightly different from those that were drawn might produce directional bias. Etching the Au too long results in underetching, giving a thinning of the Au, or even a complete loss of the Au, at the bilayer edges. Small particulates give rise to point defects, which destroy the symmetry of the bilayer and cause misfolding. During actuation, small particulates interfere with curling.

In the two additional samples (Samples 2 and 3) shown in this section, the fabrication was not as perfect as in Sample 1 (Figure SI - 7, Figure SI - 8). For example, during fabrication these

samples were exposed to acetone, which Sample 1, shown in the main text, was not, and this most likely resulted in a small degree of stiction.

The fraction of spirals for Samples 2 and 3 is shown in Figure SI - 6, in comparison with the data from Figure SI - 5. The key thing to note is that even given the defects, the fraction of bilayers bending into the spiral configuration nevertheless still increased strongly with aspect ratio. This is remarkable given the very small energy differences (less than 1%) between spirals and cigars for these aspect ratios at these strains (see Figure 2D in the main text).

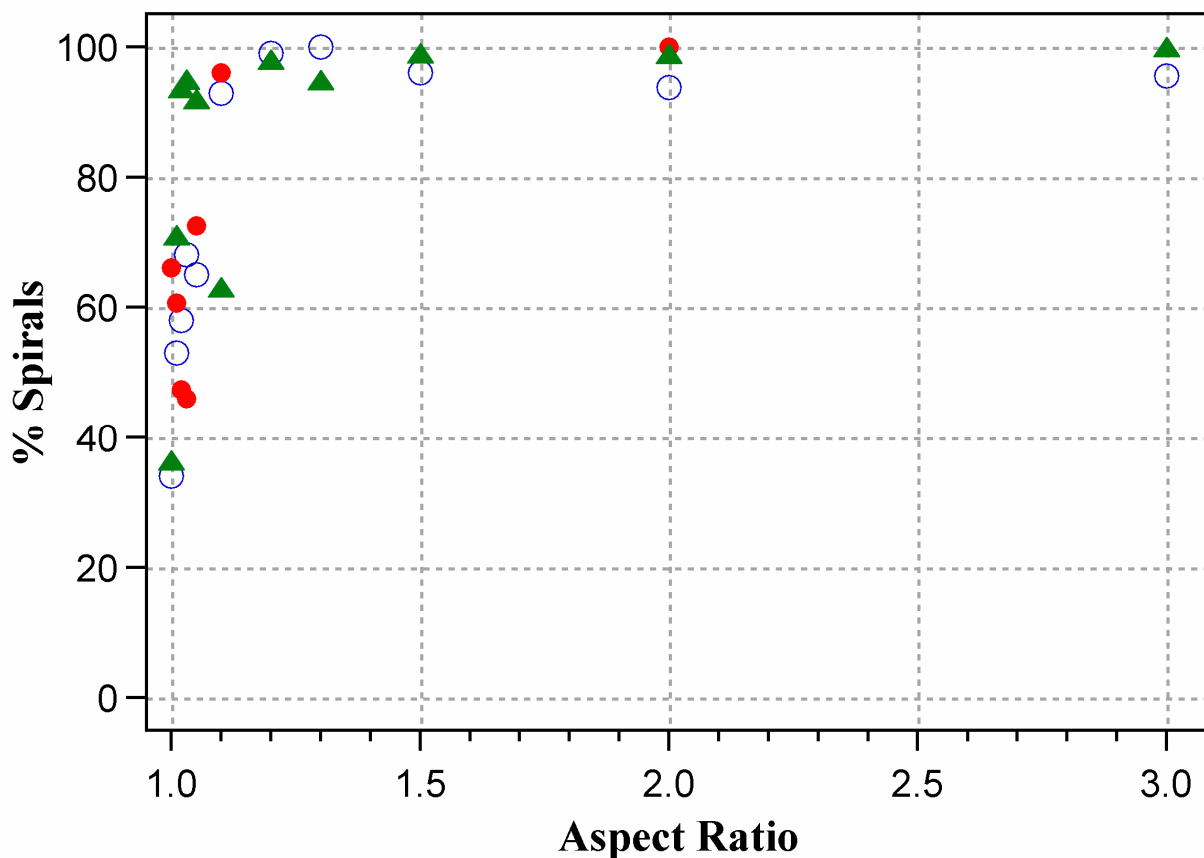


Figure SI - 6. The fraction of defect-free PPy/Au bilayers that curled into spirals as a function of aspect ratio. Open blue circles are from Sample 1, green triangles are from Sample 2, and red circles are from Sample 3.

Supporting Info for Experiments in “Edge Effects Determine the Direction of Bilayer Bending”
Alben, Balakrisnan, Smela

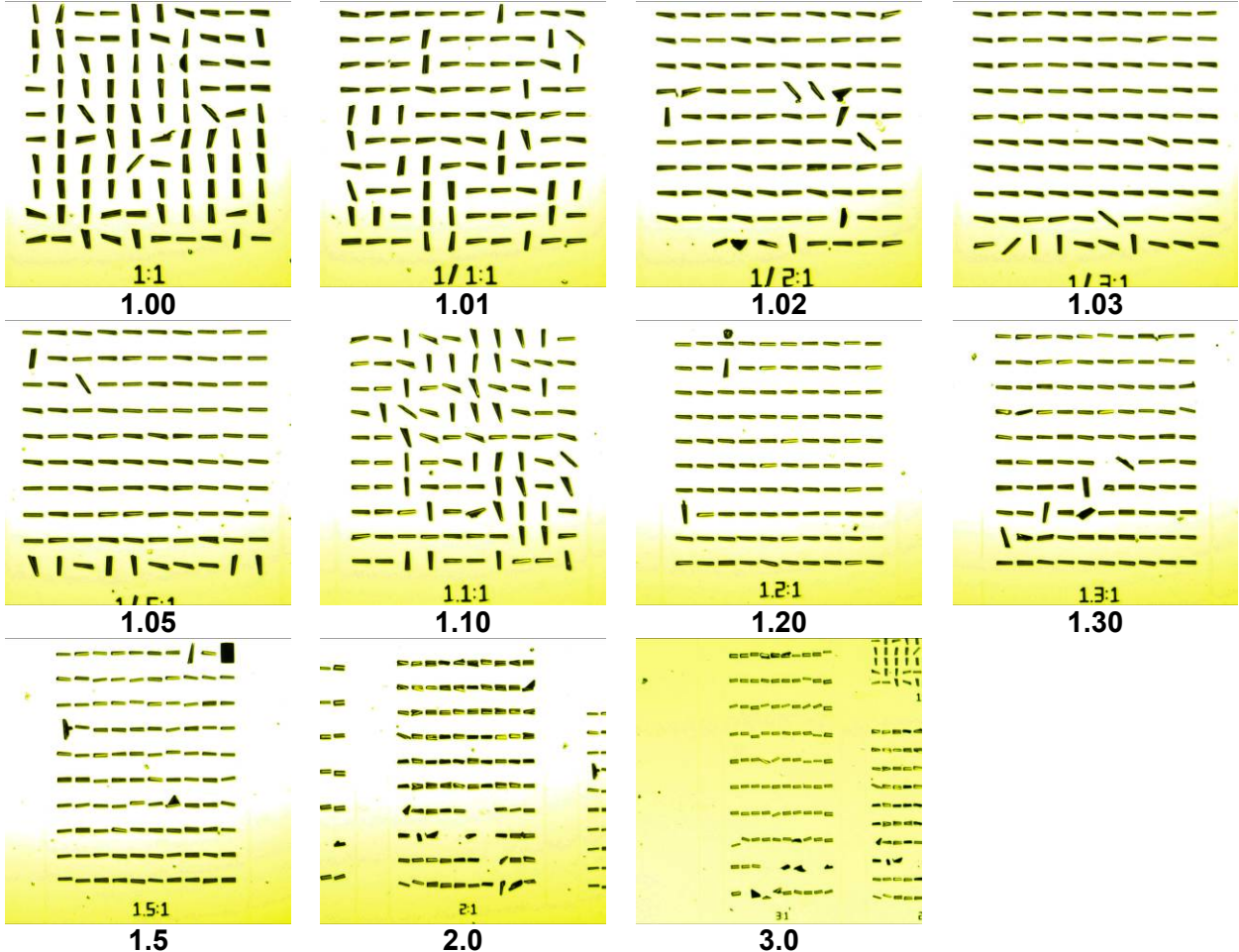


Figure SI - 7. Arrays from Sample 2 (green triangles in Figure SI - 6).

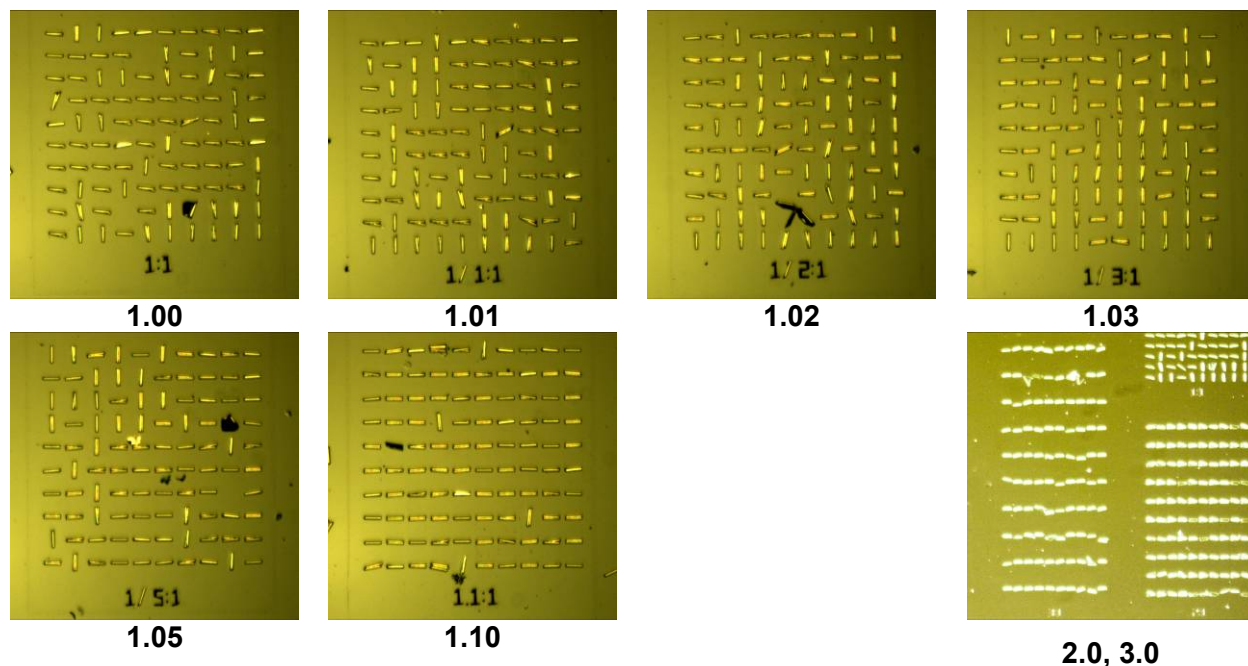


Figure SI - 8. Arrays from Sample 3 (red circles in Figure SI - 6). (The missing devices were accidentally damaged during testing.)

4 Y-Direction Bending < 50% for $A = 1$

Each of the three samples had three arrays with an aspect ratio of 1 (Figure SI - 9). In eight of these arrays, there was a preference for the bilayers to bend along either along the x -direction (samples 2 and 3) or the y -direction (sample 1), with approximately two thirds of the bilayers going one way and one third the other (Table SI - 1). Only one of these arrays showed 50% going both directions, as would be expected if there was no bias.

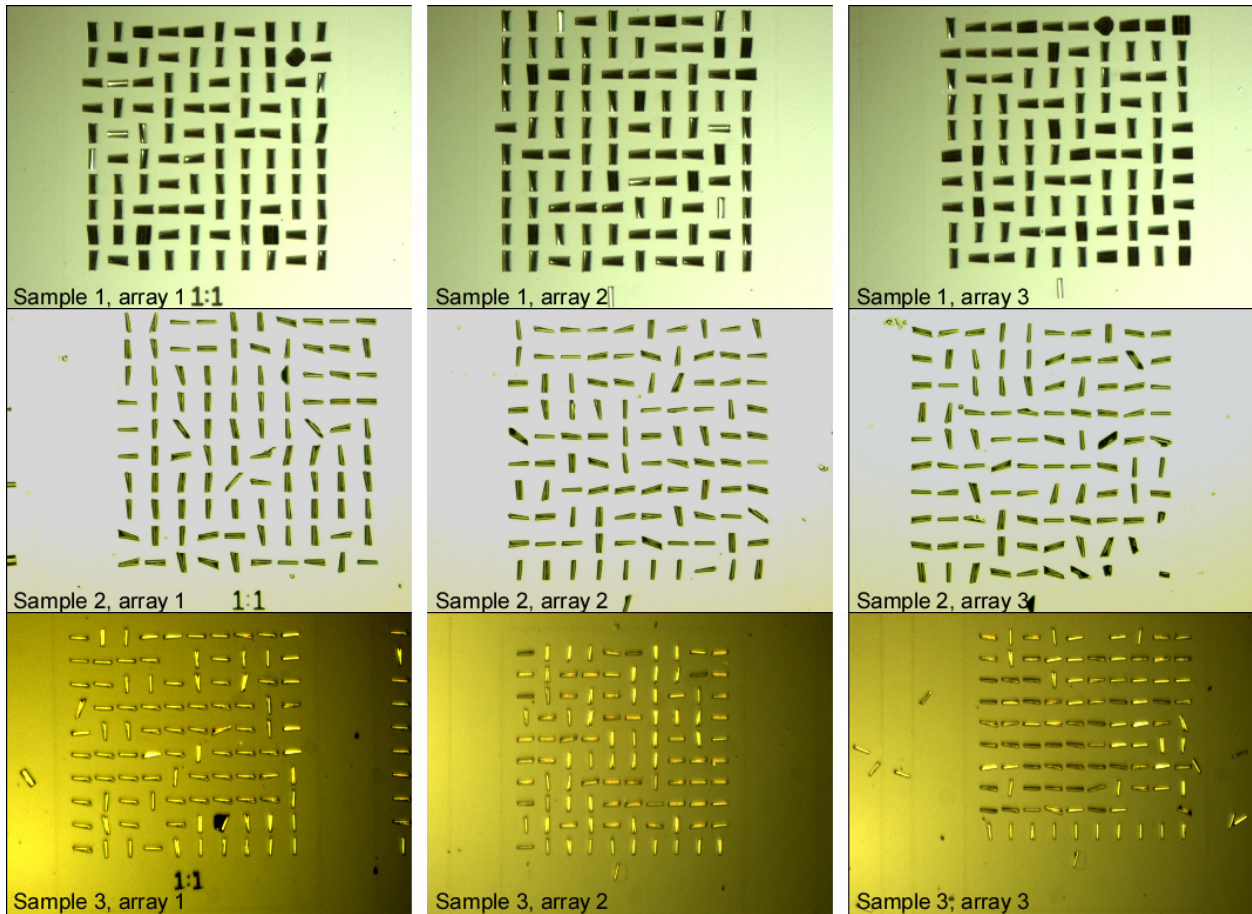


Figure SI - 9. Nine $A = 1$ arrays from three samples.

Table SI - 1. Fraction of bilayers bent into the y -direction (horizontal tubes) for $A = 1$ arrays.

Sample	Array 1	Array 2	Array 3
Sample 1	34%	34%	40%
Sample 2	35%	63%	65%
Sample 3	66%	51%	77%

The reason for the bias in these arrays is unclear. However, sample 1 was from one wafer, and samples 2 and 3 were from another wafer, suggesting that it was a difference in the fabrication process for each wafer. Given that the sample 1 arrays had a preference for x and other two a smaller preference for y , one can rule out non-square features on the photolithography mask as being responsible. However, a small tilt of the wafer relative to the mask during exposure may have produced a small foreshortening that made the bilayers not perfectly square, with the tilt being different for the two wafers. The flow of chemicals over the structures during etching may also not have been perfectly symmetric. Both wafers were dry etched at the same position and orientation in the reactive ion etcher, but agitation during the wet etch steps might have added some directionality.

Systematic thickness variations in x versus y might have been introduced by wafer placement in the evaporator, or by the placement of the counter and reference electrodes during electrochemical deposition or actuation. This seems to be an unlikely explanation for the bias, however, given the inconsistency of the results based on the array number and the difference between the two wafers. The variation in PPy thickness across the wafer was approximately 1000 Å based on film color, with the PPy being thicker at the edges of the sample than the center. This corresponds to a difference of only approximately 5 Å across a single bilayer, with the direction varying depending on the array position.

5 Square vs. Circular Center Mount

In order to examine the question of whether the shape of the center mount influenced the behavior, a mask was designed in which the top five rows of each array had a circular-shaped center mount and the bottom five rows the usual square mount.

During the fabrication of these devices, during step 1 (Figure SI - 1) the patterning of the sacrificial oxide was done 4 months after the deposition of the Cr and oxide layers, rather than immediately. These bilayers adhered slightly to the surface and didn't curl up completely freely during the first actuation cycle. As a result, a significant number of the bilayers dog-eared. This is the subject of a future paper. While it is not clear why the delay in patterning affected the bilayer release, release is strongly affected by processing procedures. (There also a small misalignment on this mask that affected the topmost row of the $A = 3$, in which the bilayers are fixed at the top.) The oxidized (curled) states are shown in Figure SI - 10 (Sample 4) and Figure SI - 11 (Sample 5).

Supporting Info for Experiments in “Edge Effects Determine the Direction of Bilayer Bending”
Alben, Balakrisnan, Smela

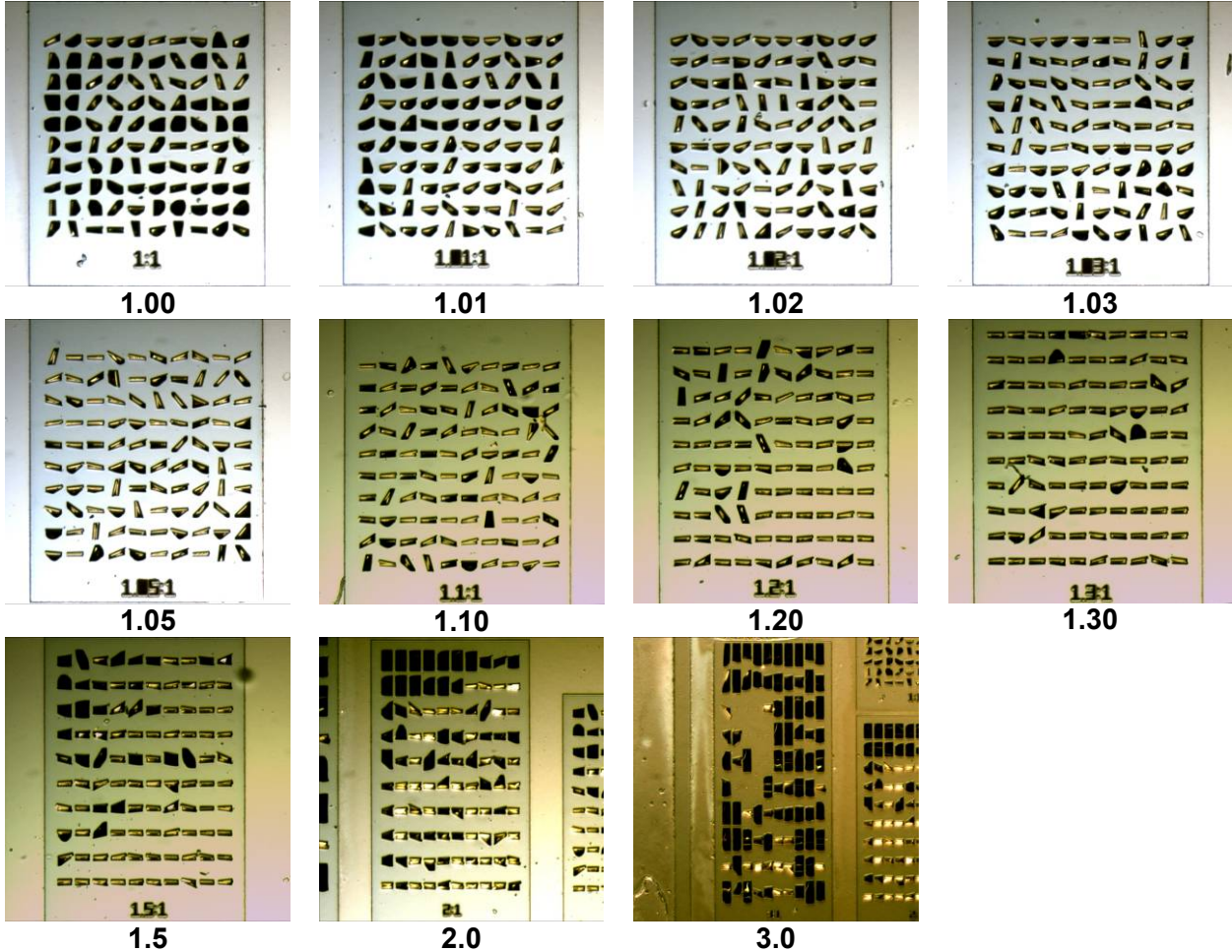


Figure SI - 10. Arrays from Sample 4 with round mounts in the top five rows of each array and square mounts in the bottom five.

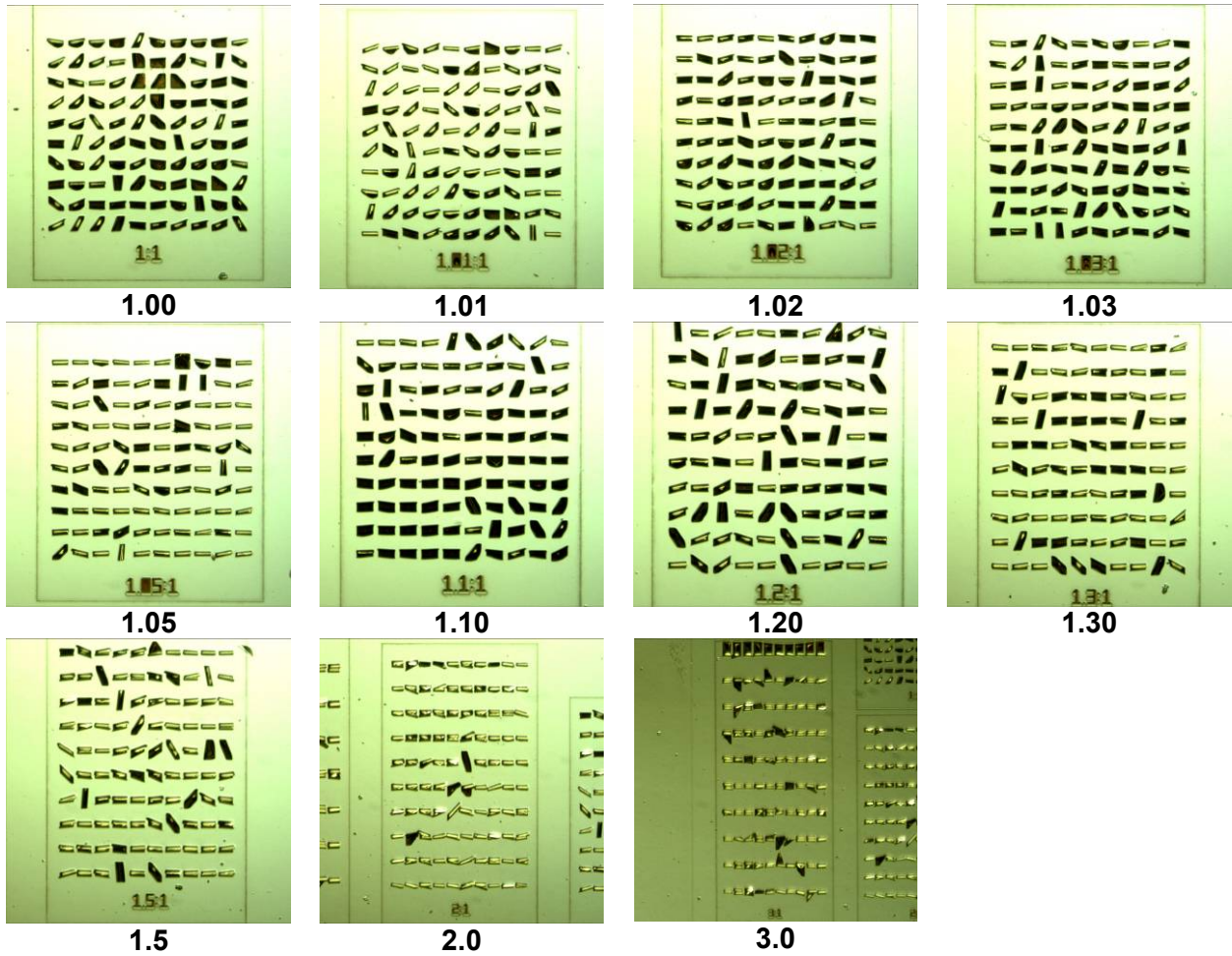


Figure SI - 11. Arrays from Sample 5 with round mounts in the top five rows of each array and square mounts in the bottom five.

The behaviors for the two mounts are compared in Figure SI - 12 and Figure SI - 13. They behaved similarly, with the number of devices curling into a corkscrew being small for both mount shapes on both samples and dropping to zero as the aspect ratio increased. We can therefore conclude that this off-axis bending is *not* due to the shape of the center mount. The fraction of bilayers bending into spirals was essentially the same for the circular and square mounts, and it increased with aspect ratio A . As discussed above, a significant number of the bilayers on Samples 4 and 5 dog-eared. For small A , the fraction of spirals was therefore small. However, as A increased, the dog-earing behavior was suppressed, in favor of the spiral configuration. These data also again show an increase in the number of defects as the area of bilayers increased.

In general, we learn from Figure SI - 12 and Figure SI - 13 that for the less perfect devices, it requires a higher aspect ratio to enforce the spiral geometry. This is consistent with the increasing energy difference with increasing A calculated in the model (Figure 2D in the main text).

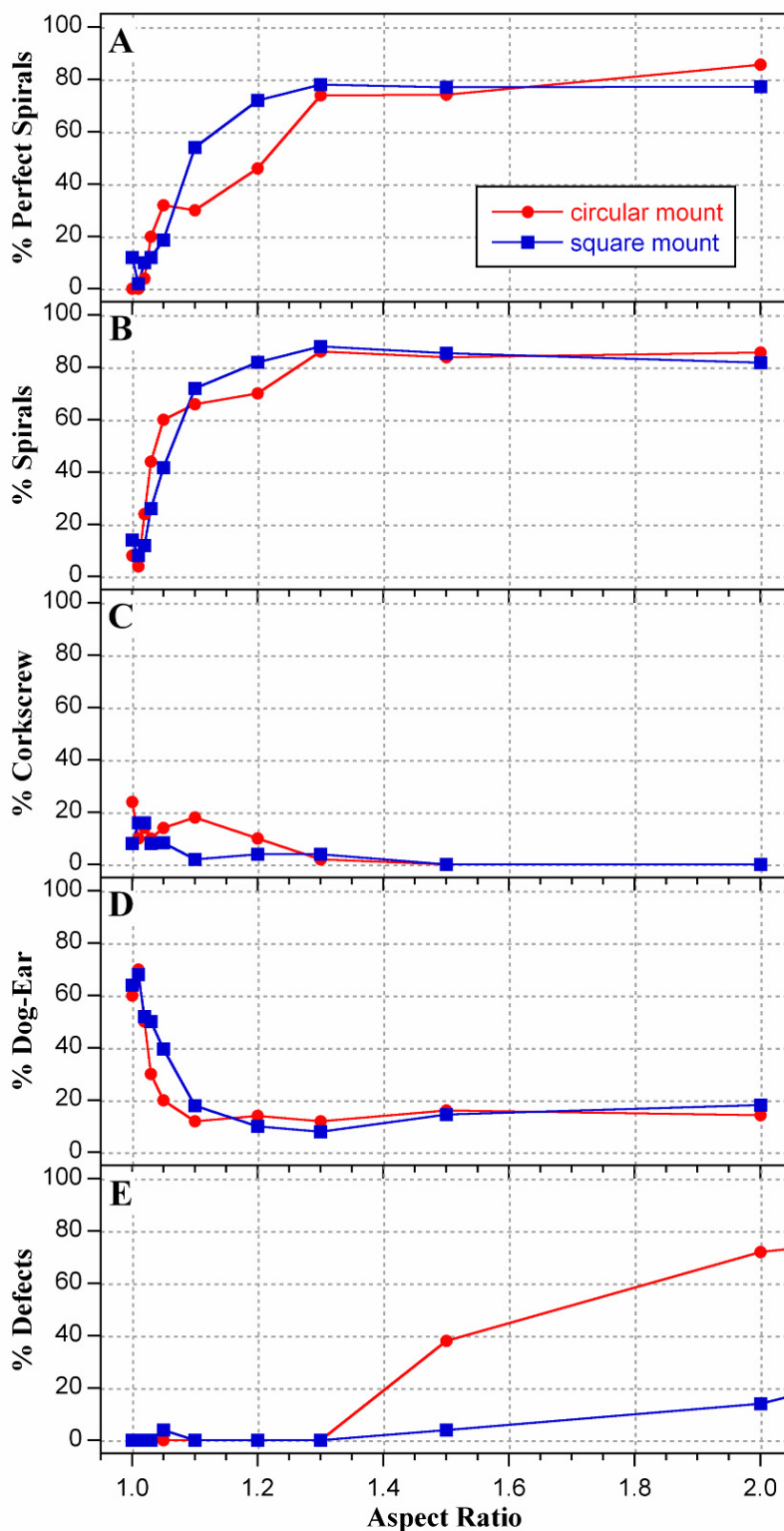


Figure SI - 12. The percentage of bilayers from Sample 4 with circular (red) and square (blue) mounts that curled into perfect spirals or spirals (all spirals, including those slightly tilted), those that curled into corkscrews, those in which at least one corner dog-eared, and bilayers that were defective.

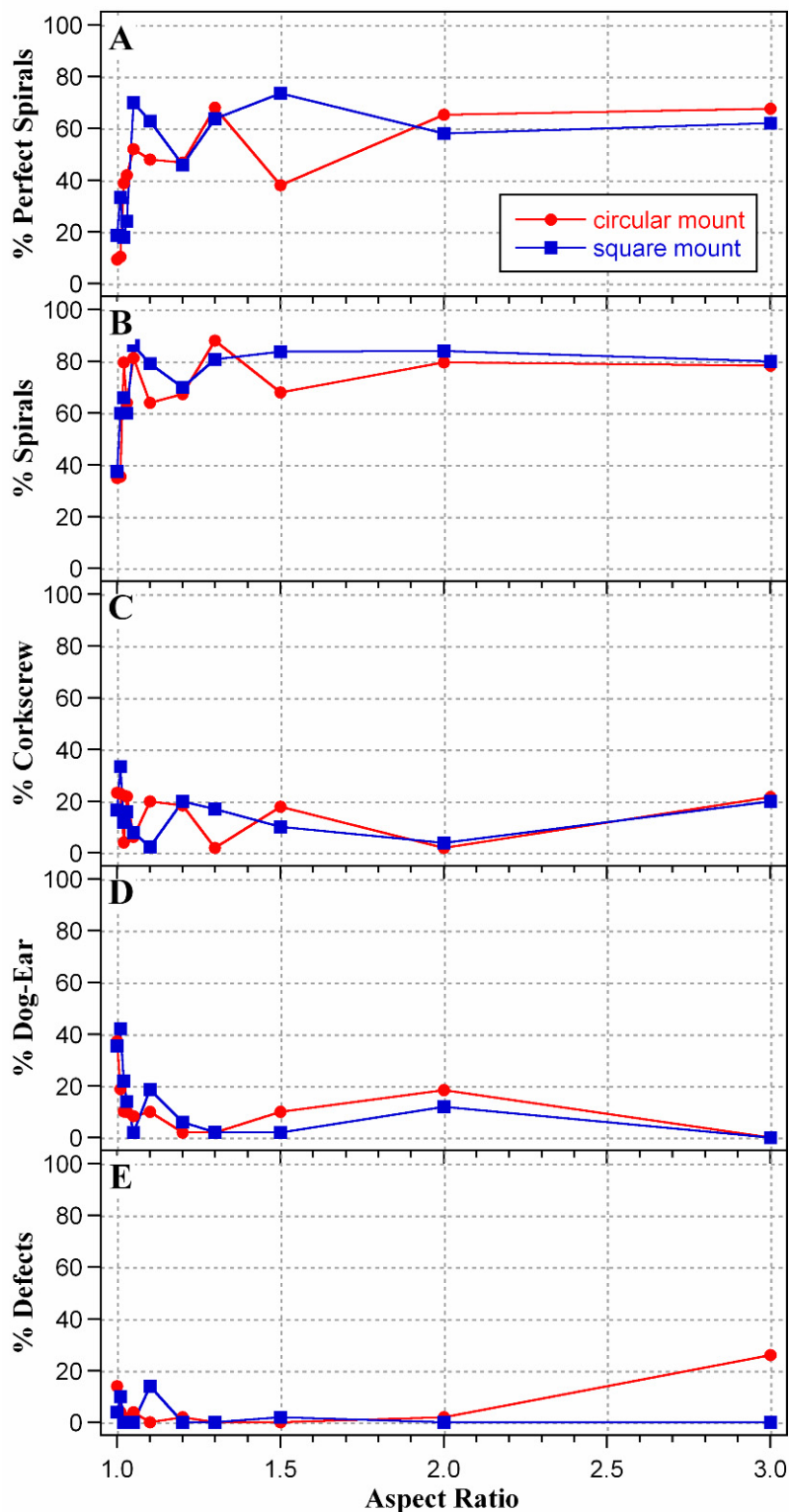


Figure SI - 13. The percentage of bilayers from Sample 5 with circular (red) and square (blue) mounts that curled into perfect spirals or spirals (all spirals, including those slightly tilted), those that curled into corkscrews, those in which at least one corner dog-eared, and bilayers that were defective.

6 Additional SEM Images

SEM images of bilayers with increasing aspect ratio are shown in Figure SI - 14, and a schematic of the curling is shown in Figure SI - 15. As the length of the bilayer increases, the only way it can curl into radius R is to form a double spiral. These were also seen in Figure SI - 3 and Figure SI - 4c,d.

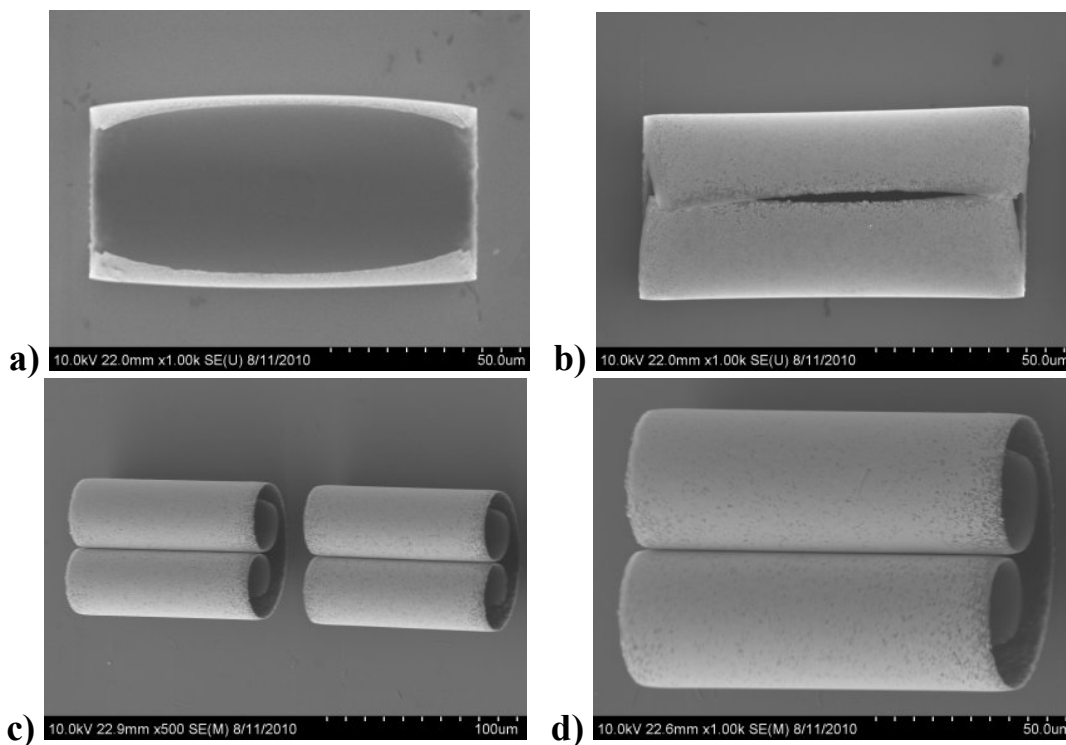


Figure SI - 14. SEM images of bilayers with aspect ratio a) 1.03, b) 1.5, c) 3.0, and d) 3.0.

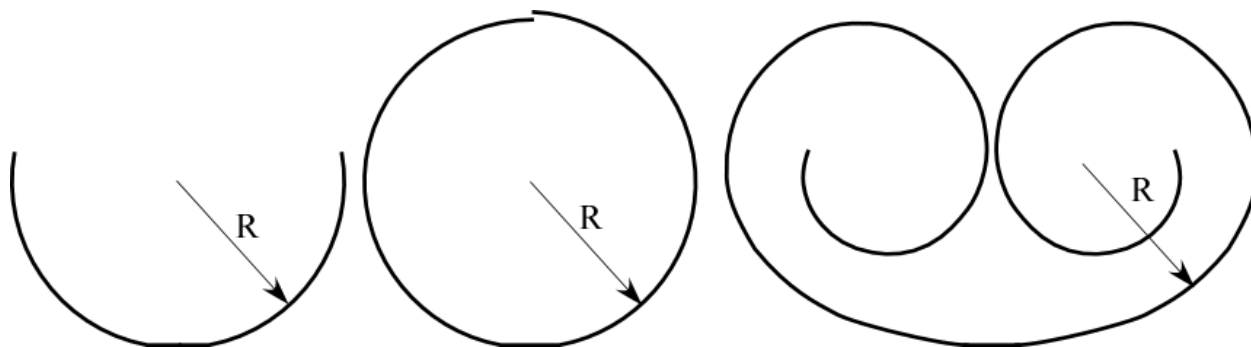


Figure SI - 15. Schematic of bilayer curling with increasing with aspect ratio (length), corresponding approximately to the images in Figure SI - 14.

7 Dog-Ears

Dog-ears were observed under two scenarios. The first was when the Au adhered slightly to the substrate, so that bilayer bending started at the edges and worked inward. This occurred when

the bilayers were made with the differential adhesion method [1,3], as illustrated in Figure SI - 16. For all aspect ratios, the corner curling was seen uniformly over the whole array.

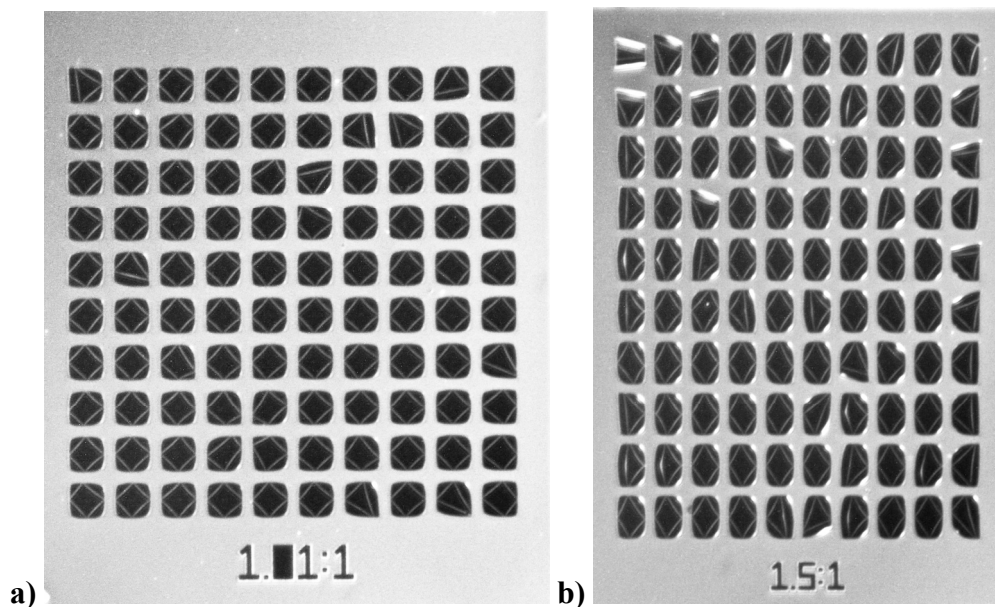


Figure SI - 16. Array of devices with aspect ratio a) $A = 1.01$ and b) $A = 1.5$ fabricated by differential adhesion rather than with a sacrificial layers, so that curling started at the corners and edges.

The second circumstance in which devices curled at an angle was when the connection to the substrate was a small bilayer hinge placed at a corner, rather than a spot in the center, as shown in Figure SI - 17. (We acknowledge Im Deok Jung for fabricating and testing these devices.)

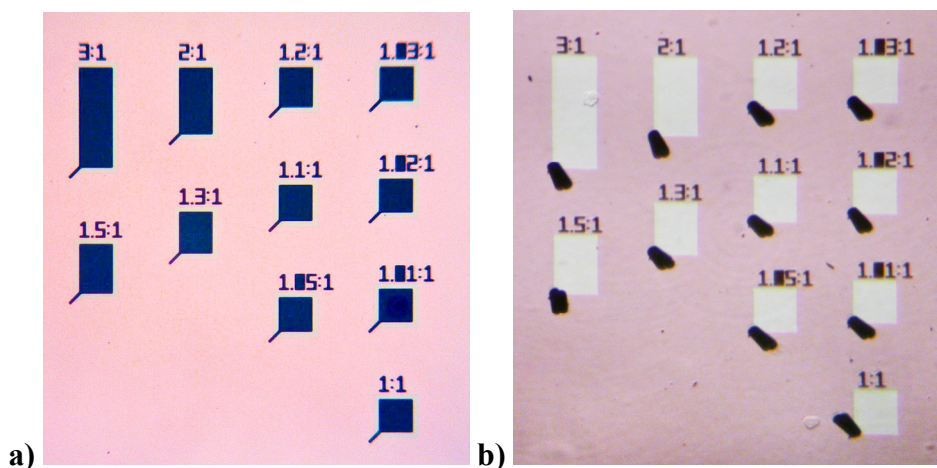


Figure SI - 17. Array of corner-mounted bilayers of varying aspect ratio a) before and b) after actuation.

8 Actuation Video

The file “Bilayer_movie_paper.wmv” is a video showing a group of bilayers with different aspect ratios actuating for the first time during cyclic voltammetry between 0 and -1 V vs. Ag/AgCl at a scan rate of 5 mV/sec. This video was made by concatenating optical images that were taken every 1 s, and it plays at 4x real time. Upon reduction of the PPy (going from 0 to -1 V), the color changed from dark to transparent, beginning at -0.85 V [4]. Upon oxidation (going back up from -1 toward 0 V), the bilayers started to curl at -0.63 V [5]. The devices chose between the spiral and cigar configurations.

Supporting Information References

1. E. Smela, "Microfabrication of PPy microactuators and other conjugated polymer devices," *J. Micromech. Microeng.*, 9, 1-18 (1999).
2. E. W. H. Jager, E. Smela, and O. Inganäs, "Microfabricating conjugated polymer actuators," *Science*, 290, 1540-1545 (2000).
3. E. Smela, O. Inganäs, and I. Lundström, "Differential adhesion method for microstructure release; an alternative to the sacrificial layer," *Transducers '95/Eurosensors IX*, Stockholm, Sweden, vol. 1, p. 218-219 (1995).
4. X. Wang, B. Shapiro, and E. Smela, "Color and volume change in PPy(DBS), Experimental studies of ion transport in PPy(DBS), Development of a model for charge transport in conjugated polymers," *J. Phys. Chem. C*, 113 (1), 359-368, 369–381, 382-401 (2009).
5. S. Shimoda and E. Smela, "The effect of pH on polymerization and volume change in PPy(DBS)," *Electrochim. Acta*, 44 (2-3), 219-238 (1998).